Preparation of a Pd/Ni Bimetallic Catalyst and its Application in the Selective Hydrogenation of Phenol

Yuze Wu*, Qingshan Xiaolu, Xuan Liu, Hongkun Tian

School of Materials Science and Engineering, Hebei University of Technology, China

*Correspondence: 202331504053@stu.hebut.edu.cn

Abstract: At present, through the coking, gasification and liquefaction of low-rank coal such as lignite and long-flame coal in industry, many low-temperature tar samples containing a high proportion of phenolic compounds can be produced. Notably, phenolic compounds are the main raw materials in the chemical industry and can be used to produce many important materials. In particular, phenolic compounds are 3~4 times more expensive than coal tar. On the basis of the importance and economy of coal tar in the production of phenolic compounds, phenol, a phenolic product of coal tar, was studied. The selective hydrogenation of phenol to cyclohexanone plays an important role in the chemical industry. The performance of phenol hydrogenation is highly correlated with the surface properties of the catalyst carrier, and good carrier selection contributes to excellent catalytic activity and stability, leading to overall process improvement in industrial-scale applications. The diversity of the structure and composition of metal oxides is conducive to the development of high-performance catalysts to promote the selective hydrogenation of phenol. Currently, supported precious metal catalysts have been widely used in the hydrogenation of phenol. Although Pd-based catalysts have improved, the loss of active sites is still an inherent shortcoming of supported catalysts, and the catalyst cost needs to be further considered. After surface modification of the ZrO_2 carrier, ascorbic acid (AA) was used to introduce a second metal to reduce the loading capacity of the precious metal Pd. The effects of adding a second metal (Fe, Co, or Ni) on the catalyst activity, hydrogenation product selectivity and stability during phenol hydrogenation were investigated. The surface physicochemical properties of the bimetallic Pd-X/ZrO_2 catalysts were investigated via XRD, XPS, NH3-TPD, H2-TPR and other characterization methods. In addition, to optimize the hydrogenation of phenol, the effects of different solvents on the catalytic performance and selectivity of cyclohexanone were further investigated.

Keywords: Phenol hydrogenation; Cyclohexanone; Ascorbic acid; Oxygen defects; Bimetal.

1. Introduction

At present, China, Vietnam, Indonesia and other developing countries have large numbers of low-rank coal resources. To make better use of these low-rank coal resources, it has been reported that low-temperature tar containing a high proportion of phenolic compounds is produced through the pyrolysis of low-rank coal such as lignite and long-flame coal. Coal tar is a complex mixture containing a variety of phenolic compounds, including phenol [1]. These phenolic compounds are highly valuable in the subsequent processing and application of coal tar but may also have adverse effects on some processes [2]. The extraction and separation of phenol from coal tar is an important research direction in the coal chemical industry. Therefore, the development of efficient and economical extraction and separation methods by many researchers also provides an efficient and feasible choice for the extraction and separation of phenol [3]. Moreover, the subsequent industrial development of phenol has also become a hot topic. Phenols have certain industrial value, and their hydrogenation products can also be used as chemical raw materials to produce different kinds of chemical products.

As a bulk chemical raw material in industry, the demand for cyclohexanone is increasing. In the past few decades, cyclohexane oxidation or phenol hydrogenation has been widely used in the industrial production of cyclohexanone. At present, most cyclohexanone in industry is synthesized from benzene, and the reaction of benzene can be carried out in two ways: complete hydrogenation and partial hydrogenation. Complete hydrogenation refers to the generation of cyclohexane (C_6H_{12}) on the Ni-based catalyst, followed by the oxidation of cyclohexane to cyclohexanone. However, this method will produce too many byproducts, resulting in a reduced yield. In addition, excessive energy consumption makes the process complicated and uneconomical [4]. Partial hydrogenation refers to the hydrogenation of benzene to cyclohexene (C_6H_{10}), followed by water and cyclohexanol ($C_6H_{12}O$) and then the dehydrogenation of cyclohexanol to cyclohexanone via Cu, Zn and other metal catalysts [5]. Compared with the benzene hydrogenation route, the selective hydrogenation of phenol to cyclohexanone has the advantages of a simple reaction route, and the reaction path of phenol hydrogenation is clearer and simpler, has mild reaction conditions and low equipment requirements, and has greater application potential. With the development of multifunctional catalysts, the interaction between metal active sites and modified components has become increasingly important. Although Pd-based catalysts have improved, the loss of active sites is still an inherent drawback of supported catalysts, and a new catalyst still needs to be conceived and manufactured to improve economic efficiency.

Nickel, cobalt and iron are the most commonly used elements in metal-based catalysts and are characterized by moderate activity and low cost. The addition of another noble metal catalyst in the form of a second metal to form an alloy or intermetallic compound with a precious metal can not only optimize the catalytic performance but also significantly improve the chemical stability of the catalyst through synergistic or electronic effects [6,7]. The addition of Ni, Co and Fe components can cause the catalyst to have magnetic characteristics, and the catalyst and reaction product can easily achieve good separation effects with the help of an external magnetic field. The experimental study revealed that the Pd/ZrO_2 catalyst modified with ascorbic acid changed the electronic state of the Pd nanoparticles on the catalyst surface, created many oxygen vacancy active sites, increased the metal–carrier interaction force, and promoted the dispersion of the active Pd metal. The surface modification of the carrier can significantly improve the performance of the selective hydrogenation of phenol to cyclohexanone. Therefore, in this work, ascorbic acid (AA) was used to modify the surface of a ZrO_2 carrier, and a series of Pd/ZrO_2+AA catalysts were prepared via the impregnation method for phenol hydrogenation to cyclohexanone. Second, the loading capacity of the modified ZrO_2 carrier for the precious metal Pd was reduced. The effects of adding secondary metals (Fe, Co, or Ni) on the catalyst activity, selectivity and stability of hydrogenation products were investigated. Active metals with different compositions, structures and properties have a large adjustable range, which can not only significantly reduce the preparation cost of the catalyst but also significantly improve the performance of the catalyst by adjusting the electronic structure of the surface active metal through interactions between bimetallic particles [8,9]. Considering the high cost of precious metals and the limitation of resources, the optimization strategy of loading bimetals on modified defective oxide carriers can provide a new direction for the design and development of stable, efficient and easy magnetic recovery catalysts in the future.

In this work, on the basis of the performance and application cost of the catalyst, the loading capacity of the precious metal Pd was reduced to 0.5%, and then the coimpregnation method was used to introduce a second metal (Ni, Co, or Fe) to prepare the bimetallic catalyst to achieve comparable or even better catalytic activity, which will provide important reference value for the efficient, green and low-cost selective hydrogenation of phenol to prepare cyclohexanone. The effects of the calcination temperature of the ZrO_2

carrier and the type and proportion of the second metal on the hydrogenation performance of phenol were investigated. XRD, XPS, H_2-TPR, and NH3-TPD were used to characterize the prepared catalyst, and the effects of introducing a second metal on the hydrogenation path of phenol and the mechanism of action of the bimetallic catalyst were explored.

2. Experimental

2.1. Materials

Anhydrous cobalt chloride, butyl acetate, ethyl acetate, titanium dioxide, silicon dioxide, gamma-alumina, ascorbic acid, urea, n-butanol, n-octanol, and phenol were purchased from Shanghai Aladdin Reagent Biochemical Technology Co., Ltd. Palladium chloride was purchased from Shanghai Dibo Biotechnology Co., Ltd. Ferric chloride hexahydrate was purchased from Shanghai Xianding Biotechnology Co., Ltd. Stannous chloride dihydrate was purchased from Shanghai Bide Medical Technology Co., Ltd. Hydrochloric acid (36.0%-38.0%) was purchased from Huanghua Century Kebo Technology Development Co., Ltd. O-Resorcinol, resorcinol and anhydrous methanol were purchased from Shanghai Yien Chemical Technology Co., Ltd. Anhydrous ethanol was purchased from Tianjin Fengchuan Chemical Reagent Technology Co., Ltd. Guaiacol was purchased from Tianjin Kelisi Fine Chemical Co., Ltd. N-decane was purchased from Tianjin Kemeiou Chemical Reagent Co., Ltd.

2.2. Catalyst preparation

Figure 1 shows that the zirconia carrier was prepared via a hydrothermal method. At room temperature, 4.8 g of zirconium oxychloride and 9.0 g of urea were dissolved in 150 ml of deionized water and stirred in a round-bottom flask for 30 minutes. The solution was then transferred to an 80 ml Teflon-lined autoclave and hydrothermally treated at 180°C for 6 hours. The white precipitate collected by centrifugation was washed with deionized water 6 times and dried overnight at 105 °C. After the dried product was ground, it was transferred to a muffle furnace and calcined at 550 °C for 6 hours, and a zirconia carrier was obtained.
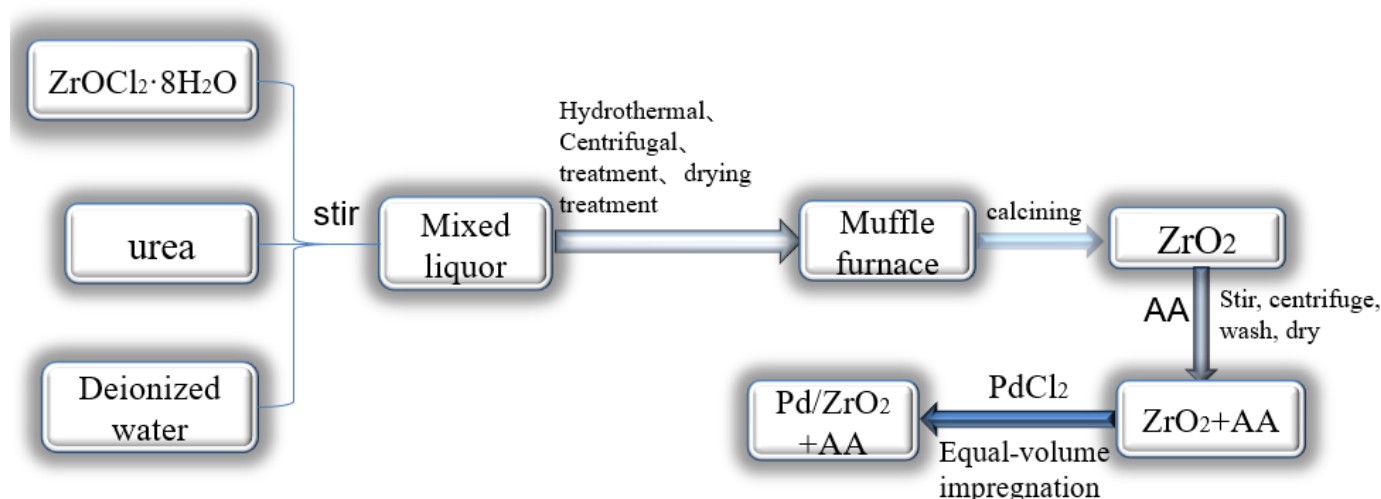

Figure 1. Preparation of the catalyst.

First, pretreatment of the ZrO_2 vector was performed. The calcined ZrO_2 powder was treated with ascorbic acid (AA). Five hundred milligrams of ZrO_2 powder was weighed and dispersed in 175 mL of distilled water, AA (176 mg, 1 mmol) was added, and the mixture was stirred vigorously at room temperature for 3 h. The resulting suspension was

divided into six equal parts, centrifuged at 8000 rpm to collect solid particles in each portion, washed four times in distilled water (30 mL each time), and dried overnight at 60 °C. The product obtained in this step was named ZrO_2+AA.

The Pd/ZrO_2+AA catalyst was then prepared via the constant volume impregnation method. The theoretical Pd metal loading capacity of the catalysts used in this study was 1 wt.%. First, an impregnation solution containing 1 wt.% Pd was prepared, and 0.0168 g of $PdCl_2$ was weighed and added to 1.8 mL of deionized water. Then, 0.6 ml of HCl (5 mol/L) was added to assist in the dissolution of $PdCl_2$. Then, 1 g of the ZrO_2+AA carrier was weighed into a beaker, and the prepared impregnation solution was added to the ZrO_2+AA carrier drop by drop. After ultrasonic treatment for 30 min, the obtained samples were put into a vacuum drying oven, dried at 40°C for 12 h, and then transferred to a blast drying oven for 2 h at 100 °C. At the end of the drying process, the sample was fully ground and then roasted continuously in a muffle furnace at 400 °C for 6h. Finally, it was reduced in a H_2 atmosphere, heated to 200 °C at 2°C/min and maintained for 2 h. Finally, the catalyst was named $1\%Pd/ZrO_2+AA$.

The ZrO_2 carrier has four calcination temperatures (450 °C, 550 °C, 650 °C, 750 °C). The calcined support was then treated with ascorbic acid, and a $Pd-X/ZrO_2+AA$ bimetallic catalyst was prepared via the impregnation method. The loading capacity of Pd was set as 0.5 wt.%, the amount of $PdCl_2$ was 0.0083 g, and the amount of zirconia carrier was 1 g. The metal salts of Ni and Pd were weighed at mass ratios of 1:2, 1:4, 1:6 and 1:8, and the metal salts of Co and Fe were weighed according to the mass ratio of Pd to X metal, which was 1:4.

The carrier was fully impregnated with salt solution and ultrasonicated for 40 min. The ultrasonic samples were placed into a vacuum drying oven, dried at 40 °C for 18 h, transferred to a blast drying oven and dried at 100 °C for 2 h. After the drying process, the samples were ground and then put into a crucible and roasted continuously in a muffle furnace at 500 °C for 6 h. Finally, they were reduced in a H_2 atmosphere, heated to 500 °C at 2°C/min and maintained for 3h. The prepared catalyst was labeled $0.5\%Pd+2\%Ni/ZrO_2+AA-T$, where T is the calcination temperature of the zirconia carrier.

2.3. Catalyst characterization

The effect of ascorbic acid modification on the surface morphology of the catalyst was investigated via transmission electron microscopy (TEM). The appropriate amount of catalyst sample was weighed and dissolved in an ethanol solution, ultrasonicated for 30 min, dropped on an ultrathin carbon film to prepare the sample, the solvent was allowed to evaporate, and the sample was tested on a machine.

The effect of the calcination temperature on the catalyst structure was analyzed via X-ray diffraction (XRD). The Cu target was used as the radiation source, the tube voltage was 30 kV, the current was 30 mA, the scanning range was 10–90°, and the scanning speed was 6°/min. After the parameters are set, the appropriate amount of sample is filled into the sample pool and then compacted into the XRD diffractometer for testing.

The influence of different types of secondary metals on the electronic states of the elements on the catalyst surface was analyzed via X-ray photoelectron spectroscopy. The binding energy data were calibrated with the binding energy of C1s (284.8 eV) as the standard, and then subpeak fitting was performed.

The influence of the introduction of the second metals Fe, Co and Ni on the surface acidity of the catalyst was analyzed via NH3-TPD. Approximately 100 mg of catalyst sample was put into the sample tube and dehydrated at 200 °C in a nitrogen atmosphere for 60 min. After the sample tube dropped to room temperature, 30 mL/min of NH_3 was absorbed and held for 30 min. The programmed temperature decoupling was set at a rate of 10°C/min to heat the reactor to 800 °C. The NH_3 concentration at each temperature point in the reactor was measured with a TCD thermal conductivity detector, and the acid con-

tent of the catalyst was measured via tail gas absorption titration. To investigate the reducibility of the catalyst and the influence of the interaction between different kinds of second metal nanoparticles and the support, the reduction of metal oxides in the catalyst was investigated via hydrogen temperature programmed reduction (H_2-TPR).

The structure and bonding of the metal oxides were investigated via Raman spectroscopy, and the defects caused by oxygen vacancies were studied. The catalyst and KBr powder were ground and mixed evenly at a mass ratio of 1:100 and then added to the pressed film to make a thin sheet with a certain diameter and thickness under pressure, after which the thin sheet was put into the instrument beam for analysis.

2.4. Catalyst test

The hydrogenation of phenol was carried out in a miniature stainless steel autoclave with phenol as the reactant (0.15 g), the catalyst (0.10 g) and n-decane (0.05 g) mixed with the solvent (10 mL). The reactor was subsequently blown with H_2 5 times and reacted for 2 h under set conditions (temperature of 120 °C, 150 °C, 180 °C, 210 °C, pressure of 0.5 MPa, 1.0 MPa, 1.5 MPa, and mechanical stirring rate of 800 rpm).

The liquid phase components were qualitatively analyzed with a Shimadzu instrument (QP2010SE) in combination with temperament (GC–MS). A Shimadzu2018 gas chromatograph (GC) equipped with an OV-1701 column (25 m×0.32 mm×0.5 μm) was used for quantitative analysis of the liquid phase components.

The product yield and selectivity for each product were calculated as follows (Formula. (1) and (2)):

$$\text{Yield}(\%) = \frac{\text{mol of product produced}}{\text{mol of phenol fed}} \times 100 \tag{1}$$

$$\text{Selectivity}(\%) = \frac{\text{mol of product produced}}{\text{mol of phenol consumed}} \times 100 \tag{2}$$

3. Results and Discussion

3.1. Catalyst characterization

The effects of different calcination temperatures on the structure of the catalyst were analyzed by X-ray diffraction (XRD). As shown in **Figure 2**, with increasing calcination temperature, the crystallinity of the carrier increases, and the intensity of the diffraction peak increases. In addition, some surface hydroxyl groups are sacrificed with increasing calcination temperature. The prepared catalyst has two weak peaks at 44.5° and 51.8°, corresponding to the (111) and (200) crystal planes of Ni [10], indicating that Ni is successfully loaded on ZrO_2. In addition, no Pd diffraction peak was observed, which was attributed to the high dispersion of Pd nanoparticles or the low metal loading content and the diffraction intensity exceeding the upper limit of machine detection. This is consistent with reports that one metal can be uniformly dispersed on the surface of another metal to form a highly dispersed bimetallic system, especially when the metal Pd load is less than 2 wt% [11]. In addition, the high dispersion of metals can expose more active sites to promote the hydrogenation rate of phenol.
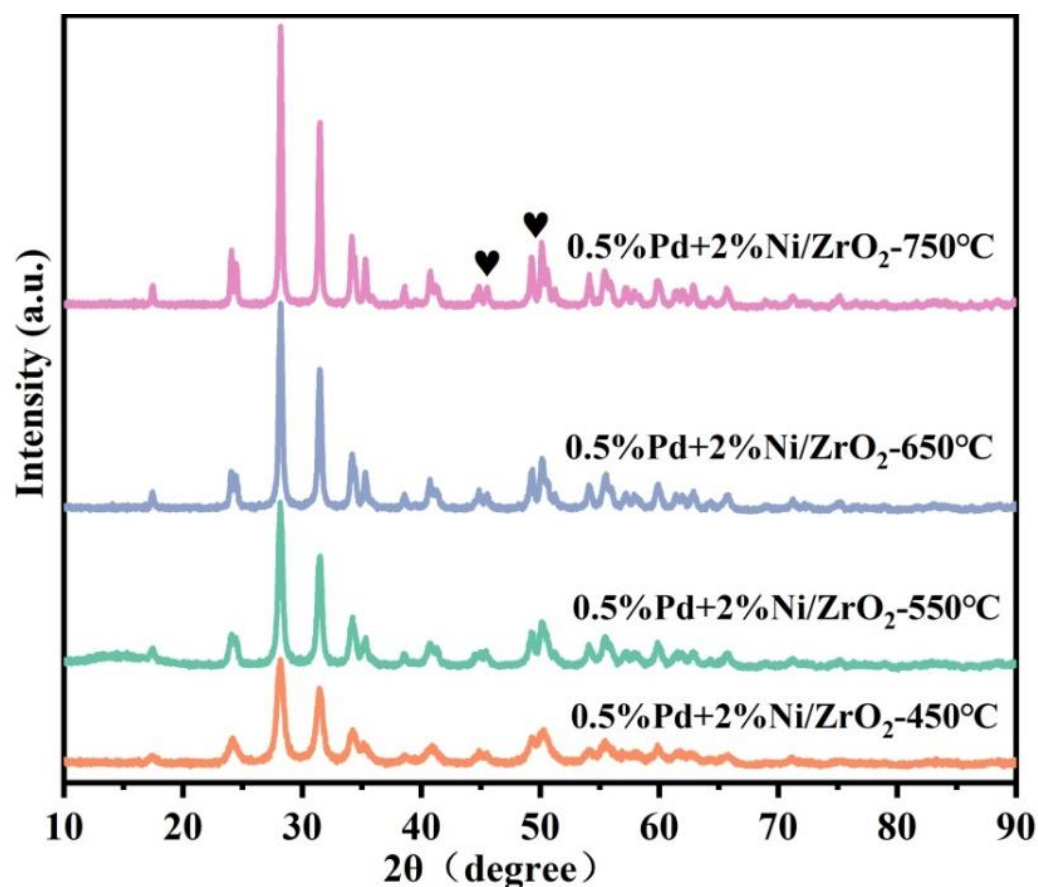
Figure 2. XRD patterns of 1%Pd/ZrO₂+AA-T.

3.1.1. X-ray photoelectron spectroscopy

The effects of different types of secondary metals on the electronic states of the catalyst surface elements were analyzed via X-ray photoelectron spectroscopy.

The peaks at binding energies of 333.92 eV and 342.51 eV were attributed to the Pd0 species. The concentration of Pd0 active sites was the highest in the Pd-Ni bimetallic catalyst, possibly because the formation of an alloy structure between Pd and Ni effectively reduced the surface fluidity of the two metals and prevented the aggregation of Pd and Ni nanoparticles. The active metal components are highly dispersed [12]. In addition, owing to the electronic synergistic effect between Pd and Ni, Ni can regulate the electronic state of the Pd atoms, thus changing the adsorption energy of the reactants and intermediates on the catalyst surface and improving the performance of the bimetallic nanocatalyst over that of the corresponding single-metal catalyst [13]. However, the addition of Co and Fe can only slightly improve or even reduce the activity of the catalyst.

In **Figure 3(a)**, the concentration of Pd^0 active sites in the Fe and Co bimetallic catalysts is low, which may be due to the geometric effect of Pd [13] coated by the second metal, which reduces the number of active sites and severely inhibits the hydrogenation rate of phenol. In addition, the close contact between Pd-Fe/Co (nonalloy) may result in a higher $Pd^0 3d_{5/2}$ binding energy, which inhibits Pd^{2+} reduction and is not conducive to phenol hydrogenation.

As shown in **Figure 3(b)**, three surface oxygen species are clearly present in the O 1 s XPS spectrum, representing lattice oxygen O_α, defect oxygen O_β and hydroxy-oxygen O_γ in the structure of zirconia. Oxygen vacancies are important active sites that can promote the adsorption and activation of oxygen-containing functional groups [14]. The oxygen vacancy concentration on the surface of Pd–Ni bimetallic catalysts is relatively high.

Therefore, the 0.5%Pd+2%Ni/ZrO₂+AA catalysts also show relatively excellent performance in the selective hydrogenation of phenol. Considering the dynamics, more surface oxygen flow may induce a phase transition. The formation of a mixed oxide phase in the catalyst prevents the surface mobility of the active metal, thereby improving the stability of the catalyst. The difference in the oxygen vacancy concentration in the different bimetallic Pd–M catalysts may be caused by the different strengths of the interactions between Pd and the second metal [15]. It is generally believed that defects can affect the charge density and surface acidity of the catalyst surface, promote the adsorption of the substrate, and thus improve the hydrogenation activity of the catalyst.
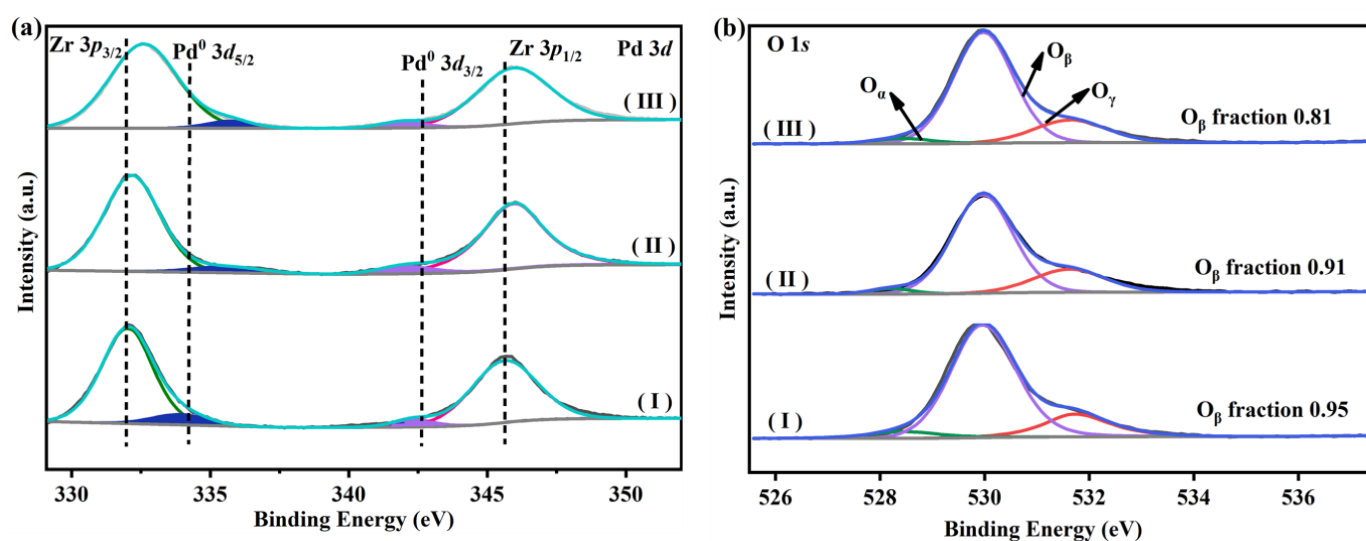

Figure 3. (a) Pd 3d XPS spectra of different bimetallic catalysts. **(b)** O 1 s XPS spectra of different bimetallic catalysts: (I) 0.5% Pd+2%Ni/ZrO₂+AA [16], 0.5% Pd+2% Co/ZrO₂+AA, (III) 0.5% Pd+2% Fe/ZrO₂+AA.

3.1.2. Reduction analysis of ammonia gas by temperature deactivation and hydrogen gas by temperature reduction

The influence of the introduction of the second metals Fe, Co and Ni on the catalyst surface acidity was analyzed via NH₃-TPD, and the results are shown in **Figure 4**. The ammonia desorption peak observed in the range of 300 °C-500 °C corresponds to the medium—strong acid center [17]. The tail gas absorption titration method was used to determine the total amount of NH3 desorbed by the catalyst during the characterization process, and the relative peak area under the NH₃-TPD curve was integrated to observe the change in total acid content on the catalyst surface. The introduction of a second metal significantly affects the concentration of acid sites on the catalyst surface. Compared with those of Ni metal, the introduction of Fe and Co results in almost no acid sites on the catalyst surface. Because of this, the selectivity of cyclohexanone is greatly reduced. The Fe and Co metals may interact with the strong acid sites on the catalyst surface to shed the acid sites, thus reducing the acidity of the catalyst.

To investigate the reductability of the catalyst and the interaction between different kinds of second metal nanoparticles and the support, the reduction of metal oxides in the catalyst was investigated via hydrogen temperature programmed reduction (H₂-TPR). The wide signal between 300 °C and 450 °C can be attributed to the strong metal–carrier interaction between the metal oxide and the zirconia support. The reduction temperature of this peak was relatively high for the 0.5%Pd+2%Ni/ZrO₂+AA catalyst, indicating that Ni oxide had a strong interaction with the metal support of ZrO₂. Strong interactions between the active metal oxide and the carrier usually lead to the reduction of the active

metal oxide at higher temperatures [18]. In addition, bimetallic alloys also have stronger interactions, which makes it more difficult to reduce them [19,20]. The stronger interaction between the nickel species and ZrO_2 is due to the presence of many low-coordination oxygen ions and defective oxygen on the surface of the carrier.
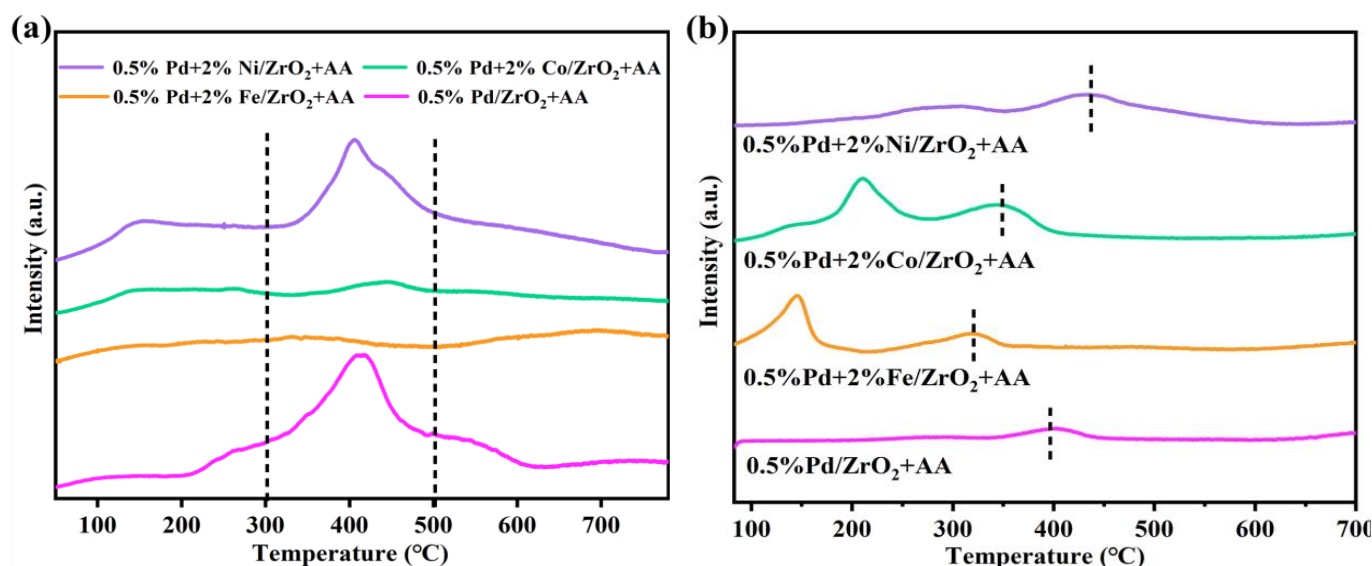

Figure 4. (a) NH_3-TPD and **(b)** H_2-TPR of different bimetallic catalysts

3.1.3. Raman and Fourier transform infrared analysis

Raman spectroscopy is sensitive to the structure and bonding of metal oxides, so it is widely used to study defects caused by doping or oxygen vacancies [21]. As shown in **Figure 5(a)**, the vibration peaks at 336 cm^{-1} and 467 cm^{-1} are due to the presence of Ni species [10]. The wide peaks at approximately 620 cm^{-1} may be caused by oxygen vacancies on the carrier surface or by the free exchange of cations [22], confirming the existence of oxygen vacancies on the catalyst surface. When the mass ratio of Pd to Ni is 1:4, the strength of the oxygen vacancy peak is slightly stronger, and the electron interaction between Pd and Ni is the greatest. As the Ni content continues to increase, the defect oxygen concentration on the catalyst surface decreases, possibly because a large amount of metal Ni will produce a geometric effect covering the active site of Pd on the catalyst surface [23], which is not conducive to electron transfer on the catalyst surface. In addition, at the defect oxygen site on the surface of ZrO_2, lower-coordination oxygen atoms are more attractive to nickel oxides, which can enhance the interaction between the support and the deposited metal, thereby improving the stability of the catalyst.

To further investigate the effects of different Ni ratios on the surface structure of bimetallic catalysts, FT-IR spectroscopy was performed to determine the oxygen-containing functional groups on the catalyst surface. As shown in **Figure 5(b)**, the peak at 3100-3750 cm^{-1} is attributed to the stretching vibration of -OH. When the mass ratio of metal Ni to metal Pd is 1:2, the vibration peak intensity of -OH is the highest, which indicates that the catalyst has the highest adsorption capacity for the phenol hydroxyl group and is conducive to improving the hydrogenation rate of phenol. In addition, the -OH group can act as an acid site, and the concentration of acid sites decreases with increasing Ni content, which is not conducive to the formation of cyclohexanone. The adsorption of phenol on the bimetallic catalyst was enhanced by the addition of Ni, and the performance of the catalyst improved.
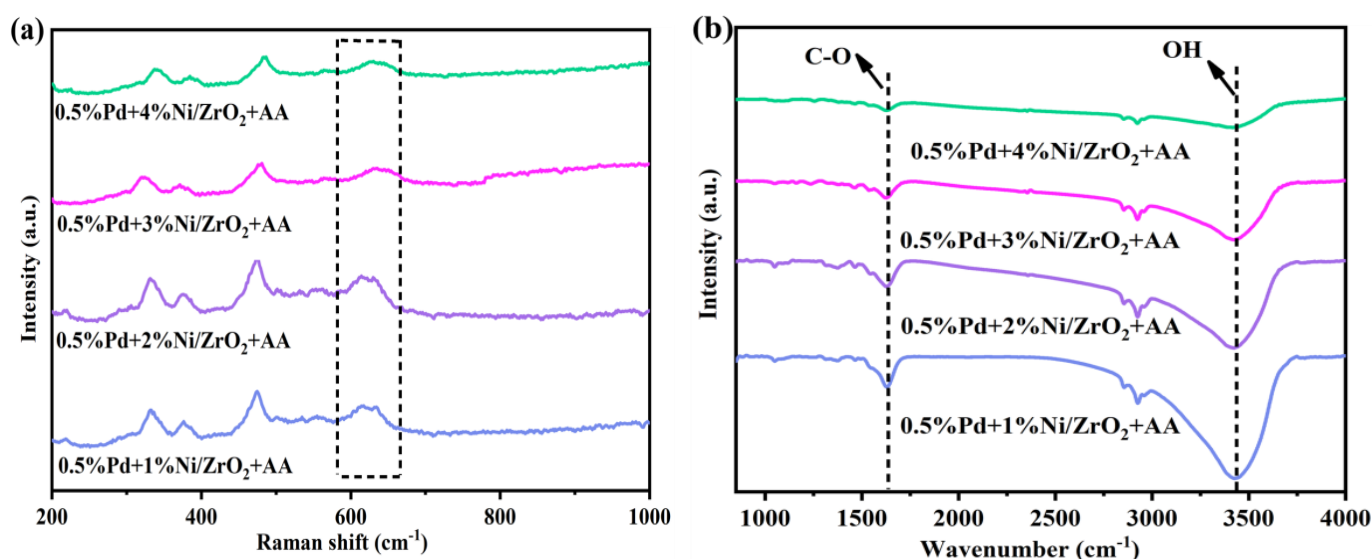
Figure 5. (a) Raman spectra of different Pd/Zr mass ratio catalysts; **(b)** FTIR spectra of different Pd/Zr mass ratio catalysts.

3.2. Catalytic activity

The effects of the introduction of different kinds of second metal components on the hydrogenation performance of phenol were evaluated, and the experimental results are shown in **Table 1**. First, when the Pd loading was reduced to 0.5%, the conversion rate of phenol decreased from 42.23% to 26.17%. There are significant differences in the conversion rate of phenol and the selectivity of cyclohexanone among different bimetallic catalysts. The addition of Ni and Co secondary metals clearly improved the conversion rate of phenol and inhibited the occurrence of side reactions (**Table 1**, items 3-5). The catalytic performance of metal Ni with the same mass fraction is better than that of Co and Fe, and $0.5\%Pd+2\%Ni/ZrO_2+AA > 0.5\%Pd+2\%Co/ZrO_2+AA > 0.5\%Pd+2\%Fe/ZrO_2+AA$, which is due to the electronic synergistic effect between Pd-Ni. It can accelerate the dissociation of H_2 molecules [13] and is more beneficial to the rapid hydrogenation process of phenol.

Table 1. Data of phenol hydrogenation on various catalysts.

Entry	Catalyst	Conversion (%)	Selectivity (%)			
			ONE	OL	MANE	DIANE
1	1% Pd/ZrO₂+AA	42.23	87.27	4.48	1.35	6.89
2	0.5% Pd/ZrO₂+AA	26.17	80.55	6.23	0.55	9.02
3	0.5% Pd+2% Ni/ZrO₂	48.69	78.86	18.27	0.33	1.35
4	0.5% Pd+2% Co/ZrO₂	29.82	61.77	30.86	1.27	2.37
5	0.5% Pd+2%Fe/ZrO2+AA	6.04	55.67	20.66	6.17	6.85
6	2% Ni/ZrO₂+AA	10.73	66.89	33.91	0.03	0.07
7	2% Co/ZrO₂+AA	7.65	54.71	39.76	0.32	0.16
8	2% Fe/ZrO₂+AA	5.48	57.96	35.66	0.86	0.23
9	0.5% Pd+2% Ni/ZrO₂	32.88	70.69	25.32	0.27	0.61

Phenol (0.15 g), catalyst (0.10 g), internal standard n-decane (0.05 g), solvent (10 ml), 1 MPa H_2, 180 °C, 2 h.

When the Ni group is introduced, the dispersion of Pd active components on the carrier surface is significantly improved, and the residence time of oxygen-containing compounds at the active site of Pd is shortened, which can reduce the formation rate of

carbon deposits [24]. Compared with the addition of Pd, the addition of Ni and Co increased the conversion rate of phenol, but the selectivity for cyclohexanone decreased. This indicates that different kinds of active metals can change the hydrogenation path of phenol. Ni and Co nonprecious metals are more likely to activate benzene rings in phenol and then directly hydrogenate to cyclohexanol [25]. The noble metal Pd is more likely to activate the phenol hydroxyl group in phenol and rapidly produce cyclohexanone after hydrogenation to ketene. The introduction of the second metal Fe does not increase the conversion rate of phenol, which may be due to the geometric effect of covering the active site of the metal Pd on the catalyst surface, which inhibits the dissociation of hydrogen molecules.

3.2.1. Effects of the calcination temperature and Pd/Ni bimetallic ratio on the catalytic performance
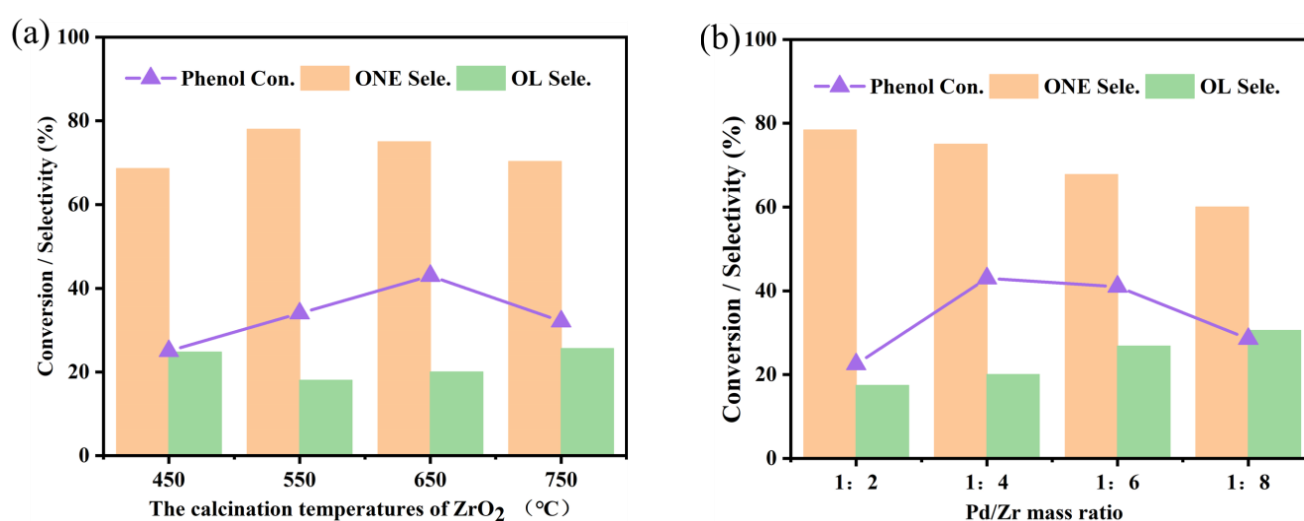

Figure 6. (a) Effect of the calcination temperature of ZrO_2 on phenol hydrogenation; (b) activity of phenol hydrogenation over catalysts with different Pd/Zr mass ratios.

Considering the conversion rate of phenol and selectivity of cyclohexanone, the Pd-Ni bimetallic catalyst has the best catalytic performance when the calcination temperature of the carrier is 650 °C, with the conversion rate of phenol reaching 46.68% and the selectivity of cyclohexanone reaching 78.46%, as shown in **Figure 6(a)**. Increasing the calcination temperature of ZrO_2 not only enhances the crystallinity of the carrier surface, which prevents the formation of oxygen vacancy defects but also sacrifices the surface hydroxyl group and reduces the adsorption capacity of phenol, thus reducing the hydrogenation rate of phenol. The reduction of the hydroxyl group on the catalyst surface means that the acid site is reduced, and further hydrogenation of cyclohexanone is more likely to occur to produce cyclohexanol. In addition, the bimetallic ratio affects the performance of the catalyst [26,27]. The bimetallic catalyst with the best catalytic performance can be obtained by changing the mass ratio of the Pd and Ni metal precursors. As shown in **Figure 6(b)**, bimetallic catalysts with different Pd–Ni mass ratios have significant differences in terms of their hydrogenation activity and product selectivity for phenol. Considering the conversion rate and selectivity of the Ni content to phenol, a ratio of 1:4 is the best. An increase in the Ni content leads to the formation of more stable structures of surface-active bimetallic Pd–Ni species (such as alloys). It has been reported that greater surface charge heterogeneity leads to enhanced interactions between the substrate and metal nanoparticles, thus reducing the activation energy of the reaction and improving the catalytic activity [28]. Moreover, the presence of Ni atoms on the surface provides an integrated effect for the catalytic process [29,30]. In a certain range, an increase in the Ni content results in Pd

being in an electron-rich state, which significantly improves the hydrogenation rate. However, excessive Ni decreases the conversion rate of phenol and the selectivity of cyclohexanone, possibly because many Ni nanoparticles cover the active site of Pd on the catalyst surface and reduce the catalytic performance. In addition, a large amount of Ni metal will lead to the formation of defect groups on the catalyst surface, which is not conducive to the desorption of cyclohexanone and further hydrogenation to cyclohexanol. Since the bimetallic catalyst showed the best catalytic performance when the mass ratio of Pd/Ni was 1:4, subsequent studies investigated the performance of 0.5%Pd+2%Ni/ZrO$_2$+AA-650.

3.2.2. Effects of reaction conditions on the hydrohydrogenation performance of phenol

In terms of the conversion rate, the influence of temperature is greater than that of pressure. With increasing temperature, the conversion of phenol increased significantly, the selectivity of cyclohexanone decreased, and that of cyclohexanol increased. However, the byproducts decrease with increasing temperature. As shown in **Figure 7(a)**, when the temperature increases from 120 °C to 220 °C, the conversion rate of phenol increases significantly from 10.89% to 70.58%, indicating that high temperature accelerates the dissociation of the phenol hydroxyl group and that the C-OH bond is more easily activated with increasing temperature [31]. The reaction temperature affects the adsorption of water and substrate by the catalyst, and the catalyst preferentially adsorbs the reactants at high temperatures. Under high H$_2$ pressure, H$_2$ molecules undergo competitive adsorption with phenyl at the active site of the catalyst, reducing the selectivity of hydrogenation products [32]. In **Figure 7(b)**, with increasing pressure, the solubility of H$_2$ molecules in the solvent improves, which increases the relative concentration of hydrogen molecules in the reaction process. However, owing to the limited number of active metals available for the active dissociation of hydrogen molecules, the hydrogenation rate of phenol has not significantly improved. Excessive pressure forces the reaction forward, resulting in an increase in byproducts. With increasing pressure, the amount of cyclohexanol gradually increased, resulting in a decrease in the selectivity of cyclohexanone.
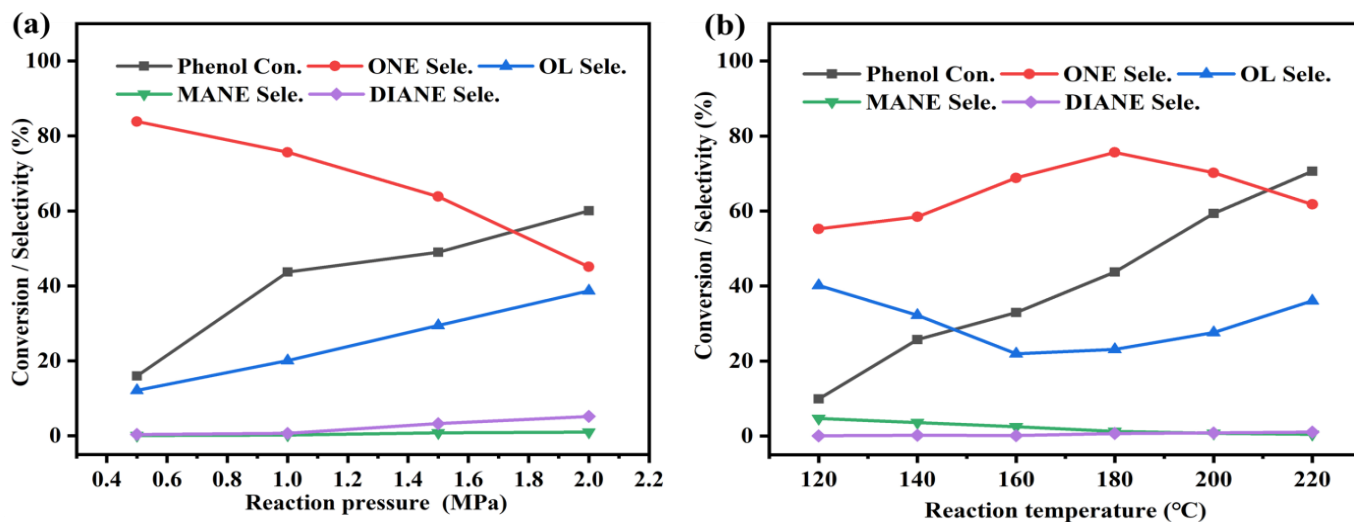

Figure 7. Effects of reaction temperature **(a)** and reaction pressure **(b)** on phenol hydrogenation. Reaction conditions: phenol (0.15 g), 0.5% Pd+2% Ni/ZrO$_2$+AA-650 (0.10 g), water/methanol (2/8 mL), 2 h.

3.2.3. Stability and universality testing of the catalysts

Compounds containing phenolic hydroxyl groups were selected to evaluate the universality of the catalyst, and guaiacol, catechol and resorcinol were used as reaction substrates. The results are shown in **Table 2**. The conversion rate of guaiacol and resorcinol

can reach more than 60%. Therefore, the modified Pd–Ni bimetallic catalyst has wide application prospects in the improvement of phenolic hydrogenation. In addition, the recyclability of a catalyst is the most intuitive key to ensure its stability [33]. As shown in **Figure 8(a)**, the 0.5%Pd+2%Ni/ZrO₂+AA-650 catalyst still exhibited excellent catalytic activity after six cycles, and the selectivity for cyclohexanone decreased slightly. In **Figure 8(b)**, the XRD patterns of the fresh catalyst and used catalyst show significant differences in diffraction peak intensity, which may be caused by the fact that some reaction products remain on the surface of the used catalyst and are not washed clean or that the interaction between the Ni-Pd metals is weakened during the process of catalyst regeneration, and the metal particles are enriched and then fall off. By adding Ni, the activity and stability of Pd-based catalysts can be improved. The strong interaction between Pd and Ni can reduce the formation of coke, which plays an important role in improving the stability of the catalyst.
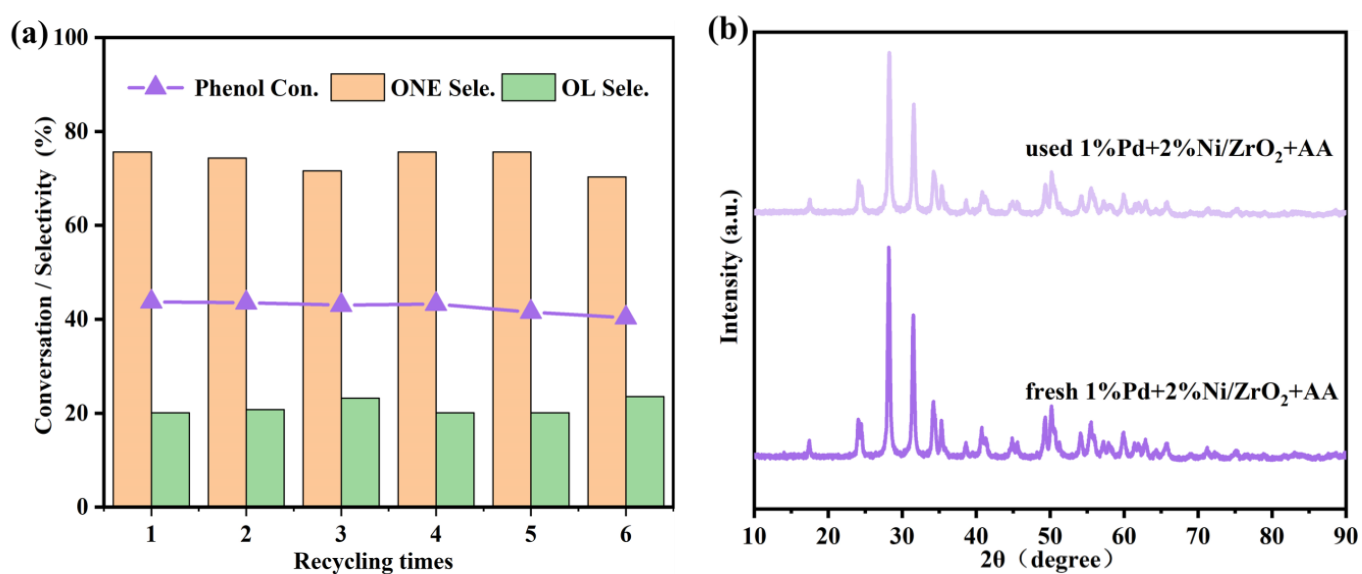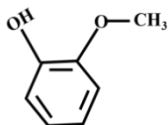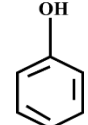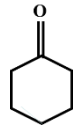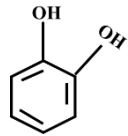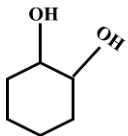

Figure 8. (a) Recyclability of 0.5% Pd+2% Ni/ZrO₂+AA-650 for phenol hydrogenation; **(b)** XRD patterns of the used catalyst. Reaction conditions: phenol (0.15 g), 0.5% Pd+2% Ni/ZrO₂+AA-650 (0.10 g), 1 MPa H₂, 180°C, 2h, water/methanol (2/8 mL).
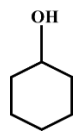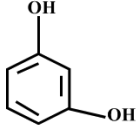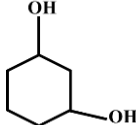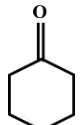
Table 2. Exploration of the universality of 0.5%Pd+2%Ni/ZrO₂+AA-650 a.

Entry	Reactant	Conversion (%)	Product	Selectivity (%)	Product	Selectivity (%)
1	(2-methoxyphenol)	75.4	(phenol)	67.4	(cyclohexanone)	16.3
2	(catechol)	40.2	(1,2-cyclohexanediol)	36.9	(cyclohexanol)	15.7
3	(resorcinol)	61.9	(1,3-cyclohexanediol)	43.6	(cyclohexanone)	25.3

a Reaction conditions: phenol (0.15 g), catalyst (0.10 g), internal standard n-decane (0.05 g), solvent (10 mL), 1 MPa H₂, 180 °C, 2 h.

3.4. Solvent effect

The solvent effect can significantly affect the catalyst activity. The phenol hydrogenation activities of the 0.5%Pd+2%Ni/ZrO$_2$+AA-650 catalysts in different solvents were compared, and the results are shown in **Figure 9**. A comparative study revealed that the stronger the polarity of the solvent was, the better the conversion effect of phenol hydrogenation. The selectivity of cyclohexanone was as high as 77.46% in the mixed solvent of water and methanol, and the conversion of phenol was as high as 88.97% in the mixed solvent of water and ethanol. Polar solvents are beneficial for phenol enrichment and affect phenol adsorption and diffusion on the catalyst surface. In summary, the mixed solvents of water and methanol result in high selectivity and a high conversion rate, which benefits from the good dispersion of the catalyst in polar solvents. Solvents can not only improve the dispersion of the reactants to enhance the mass transfer process in the catalytic reaction but also change the reaction process kinetically [34]. Studies have shown that a polar solvent has a better hydrogenation effect than a nonpolar solvent because the dispersion of the catalyst is uniform, which strengthens the mass transfer and diffusion between the catalyst and reactant and makes the reaction move forward [33].

As shown in **Figure 9**, with increasing carbon number in alcohol, the conversion rate of phenol decreases, and the selectivity of cyclohexanone also tends to decrease. The conversion rate of phenol decreased from 46.68% to 18.32%, and the selectivity of cyclohexanone decreased from 78.46% to 48.67%. With increasing carbon number in the solvent, the viscosity of the solvent also increases, which leads to poor diffusivity of the reactants and products, which is one of the reasons for the poor hydrogenation effect of alcohols with high carbon numbers. The stronger the polarity of the solvent is, the better the conversion effect of phenol hydrogenation, which is affected mainly by the hydrogen bond donor capacity (i.e., Lewis acidity) and hydrogen bond acceptability (i.e., Lewis alkalinity) [35]. The shorter the carbon chain of the fatty alcohol is, the stronger the hydrogen bond between the carbonyl oxygen of cyclohexanone and the hydroxyl of the solvent [36], which is more conducive to the timely desorption of cyclohexanone on the catalyst surface.
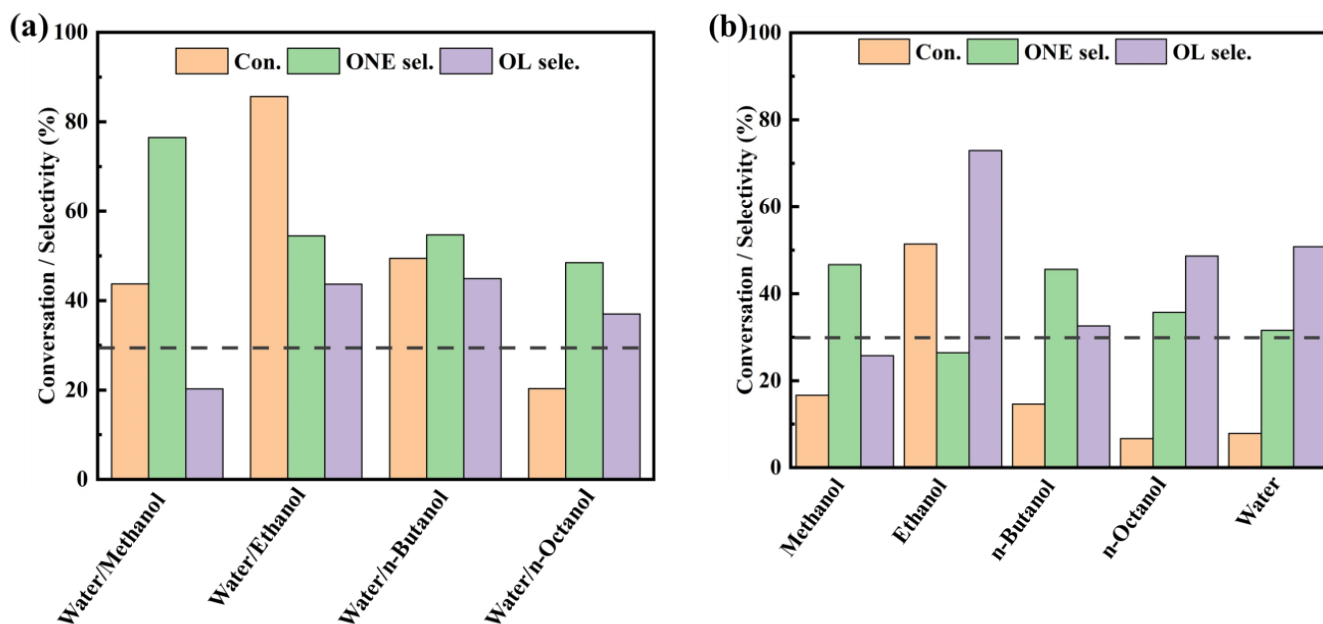

Figure 9. Effect of the reaction temperature **(a)** and reaction pressure **(b)** on phenol hydrogenation. Reaction conditions: phenol (0.15 g), 0.5% Pd+2% Ni/ZrO$_2$+AA-650 (0.10 g), solvent (10 mL), 2 h, 180°C.

This hydrogen bonding force is most pronounced when only methanol is present in the reaction solvent, which reduces further hydrogenation of intermediates containing C-O. The strong interaction between phenol and methanol in the solvent reduces the adsorption of cyclohexanone on the catalyst surface, which leads to rapid separation of cyclohexanone from the catalyst and inhibits its excessive hydrogenation to cyclohexanol. However, in alcohol-only solvents, alcohol dehydrogenation is preferred at any temperature, followed by self-etheration or dehydration to alkenes and then hydrogenation to alkanes at high temperatures [37]. Therefore, compared with a pure alcohol solvent, a solvent with an appropriate water and alcohol ratio results in moderate interactions between the reactant and catalyst, which can reduce the activation energy barrier of the intermediate product and is more conducive to the selective hydrogenation of phenol.

Compared with water/alcohol solvents, water/ester biphase solvents significantly differ in the selective hydrogenation of phenol. As shown in **Table 3**, when the ratio of water to butyl acetate was 2:8, the conversion of phenol reached 67.08%, and the selectivity of cyclohexanol reached 72.2%. The water/ester biphase solvent is more beneficial for the production of cyclohexanol. Through a literature review and comprehensive consideration, butyl acetate was selected as the oil phase [38] to further explore the effect of the ratio of butyl acetate to water in the solvent on the selectivity of cyclohexanone. With increasing water content in the solvent, the selectivity of cyclohexanone decreases sharply, and the presence of a large amount of water is more likely to lead to the hydrogen transfer process, resulting in excessive hydrogenation of phenol to cyclohexanol [39]. When the ratio of water to butyl acetate was 1:1, the conversion of phenol reached 94.87%, and the selectivity of cyclohexanone showed a turning point. The difference in the hydrogenation products may be due to the different solubilities of phenol, cyclohexanone and cyclohexanol in water and butyl acetate. By analyzing the experimental results, a higher conversion rate of phenol (54.55%) and a higher selectivity of cyclohexanone (63.15%) can be achieved by choosing a solvent with a ratio of water to butyl acetate of 7:3. Moreover, fewer byproducts are produced in the hydrogenation process of phenol under these conditions.

Table 3. Phenol hydrogenation effects on different ratios of water/butyl acetate a.

Entry	Water/butyl acetate (mL/mL)	Conversion (%)	Selectivity (%)			
			ONE	OL	MANE	DIANE
1	0/10	44.67	40.74	58.78	0.19	0.04
2	1/9	49.86	32.64	63.01	0.24	0.18
3	2/8	67.08	27.42	72.22	0.31	0.21
4	3/7	54.38	28.31	71.63	0.36	0.14
5	4/6	85.96	7.48	92.41	0.37	0.02
6	5/5	94.87	2.24	97.51	0.42	0.03
7	6/4	77.88	56.22	43.77	0.73	1.01
8	7/3	54.55	63.15	36.49	0.94	2.85
9	8/2	40.15	49.23	42.36	1.36	6.31
10	9/1	23.01	40.67	45.71	2.47	6.74
11	10/0	7.89	31.59	50.78	3.62	7.89

a Reaction conditions: phenol (0.15 g), 0.5% Pd + 2% Ni/ZrO$_2$+AA-650 catalyst (0.1 g), n-decane (0.05 g), solvent (10 mL), 1 MPa H$_2$, 180°C, 2h.

3.5. Catalytic mechanism

On the basis of the characterization analysis and experimental results of the catalyst, the electronic synergistic effect between Pd and Ni can improve the exposure of the active site to the substrate, making the performance of the bimetallic nanocatalyst better than that of the Pd-based monomeric catalyst. The addition of the second metal Ni will cause

the surface charge of the catalyst to be uneven, forming oxygen defects on the ZrO_2 support to keep the charge neutral. Although the detailed chemical composition of defects in oxides is complex, the effect of doped secondary metals on the chemisorption capacity of catalysts is very large. The concentration of defect oxygen usually increases with increasing content of doped Ni. Once a certain level of doping is reached, a defect group may be formed, which is not conducive to the adsorption of substrates and the separation of intermediates. In addition, with increasing Ni content, more metal Ni oligomers are deposited on the surface of Pd nanoparticles, which, to a certain extent, hinders contact between the reaction substrate and the hydrogenation site, leading to a decrease in activity [15]. The interaction between the Pd–Ni alloy and support leads to the structural characteristics of electron deficiency on the catalyst surface and the formation of p-π interactions between -OH, which acts as the acid site in the support, and the benzene ring, which increases the electron density of the benzene ring. Carbon–carbon double bonds with high electron density are easier to attack, which can significantly reduce the activation energy of the reaction, thus improving the catalytic performance. In the hydrogenation of phenol, the phenol hydroxyl group is more likely to dissociate on the surface of a catalyst containing defective oxygen, whereas the mutual alteration of ketene is more likely to occur on the surface of a metal catalyst. The selectivity difference of cyclohexanone depends on the difficulty of further hydrogenation of cyclohexanone. In addition, the adsorption capacity of the phenol hydroxyl group on the Ni metal surface is much weaker than that of the benzene ring, and the direct hydrogenation of phenol more easily produces cyclohexanol, reducing the selectivity of cyclohexanone [25].

According to the above analysis, the possible mechanism of phenol hydrogenation on the 1%Pd+2%Ni/ZrO_2+AA catalyst is shown in **Figure 10**. Phenol is adsorbed on the coordination unsaturated metal site (Zr^{4+} cation) on the oxide surface to form phenoxy ions that interact with Ni, which is conducive to the hydrogenation of the benzene ring. After partial hydrogenation of the phenyl ring of phenol to form an enol, it can be rapidly isomerized to obtain cyclohexanone by combining with active H at the interface site of Pd–Ni. There is a weak H bridge donor on the catalyst surface, and the adsorbed and bonded new phenol molecules replace cyclohexanone so that cyclohexanone quickly leaves the catalyst surface and avoids further hydrogenation to cyclohexanol. The formation of active hydrogen species at metal sites is highly dependent on the probability of hydrogen adsorption and the electronic interaction between hydrogen and metal particles [39]. Ni doping further increases the concentration of these active H species and forms a H bridge donor at the interface site of Pd–Ni to protect cyclohexanone from further hydrogenation.
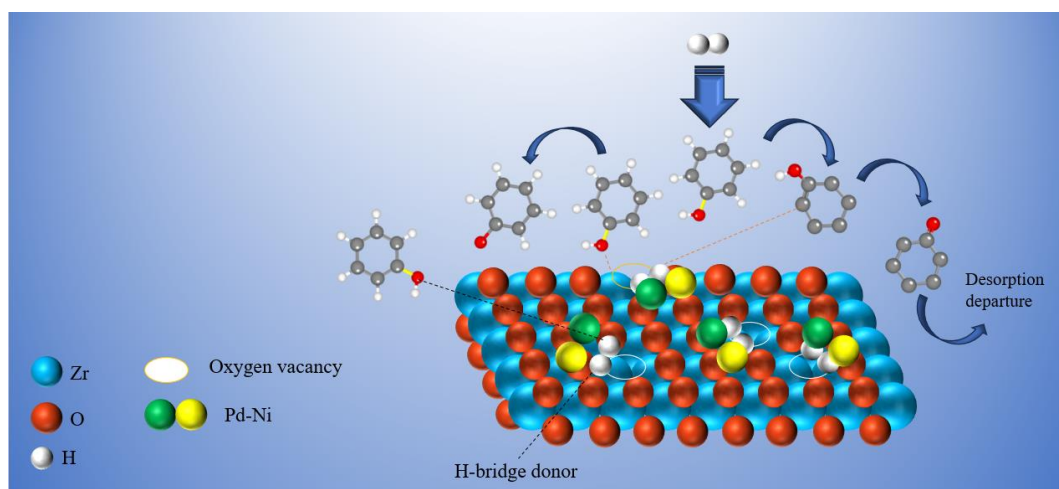

Figure 10. Reaction route of phenol hydrogenation over the Pd–Ni bimetallic catalyst.

4. Conclusion

Bimetallic catalysts with low Pd (0.5 wt.%) loading capacity were prepared by adding Fe, Co and Ni, and their effects on the hydrogenation performance of phenol were investigated. The bimetallic Pd–Ni catalyst showed excellent hydrogenation performance. The aggregation of Fe and Co leads to a decrease in the concentration of Pd^0 active sites and acid sites on the bimetallic catalyst surface, which leads to a decrease in phenol conversion and cyclohexanone selectivity. The addition of Ni can increase the charge density and surface acidity of the catalyst surface, promote the adsorption of the substrate, and improve the hydrogenation activity of the catalyst due to the electronic synergism between Pd and Ni. The formation of active hydrogen around metal sites is also highly dependent on the probability of hydrogen adsorption and the electronic interaction between hydrogen and the metal. The electronic synergism between Pd-Ni is more likely to activate active H, and the high concentration of active hydrogen species on the catalyst surface can form H-bridge donors to promote the adsorption of phenol and the desorption of cyclohexanone. In addition, the content of nickel can affect the performance of palladium-based catalysts. The optimal mass ratio of Pd/Ni is 1:4. The introduction of nickel metal redistributes electrons on the catalyst surface, increases the charge density on the catalyst surface, generates more oxygen defects, and promotes the adsorption and activation of phenol.

Nomenclature

AA, ascorbic acid; H_2-TPR, temperature-programmed reduction of H_2; FT-IR, Fourier transform infrared spectroscopy; TEM, transmission electron microscopy; NH_3-TPD, temperature-programmed desorption of NH_3; XRD, X-ray diffraction; XPS, X-ray photoelectron spectroscopy.

References

1. Meng, H., Ge, C. T., Ren, et al. Complex extraction of phenol and cresol from model coal tar with polyols, ethanol amines, and ionic liquids thereof. Industrial & Engineering Chemistry Research, 2014, 53(1), 355-362. https://doi.org/10.1021/ie402599d
2. Shi, H., Liu, Y., Song, J., et al. On-surface synthesis of self-assembled monolayers of benzothiazole derivatives studied by STM and XPS. Langmuir, 2017, 33(17), 4216-4223. https://doi.org/10.1021/acs.langmuir.7b00674
3. Chen, H., Sun, J. Selective hydrogenation of phenol for cyclohexanone: A review. Journal of Industrial and Engineering Chemistry, 2021, 94, 78-91. https://doi.org/10.1016/j.jiec.2020.11.022
4. Pérez, Y., Fajardo, M., Corma, A. Highly selective palladium supported catalyst for hydrogenation of phenol in aqueous phase. Catal Commun, 2011, 12 (12), 1071-1074. https://doi.org/10.1016/j.catcom.2011.03.026
5. Shanjun, M., Zhe, W., Qian, L., et al. Geometric and electronic effects in hydrogenation reactions. ACS Catalysis, 2022, 13(2), 974-1019. https://doi.org/10.1021/acscatal.2c05141
6. Yan, B., Zhao, B., Kattel, S., et al. Tuning CO_2 hydrogenation selectivity via metal-oxide interfacial sites. Journal of Catalysis, 2019, 374, 60-71. https://doi.org/10.1016/j.jcat.2019.04.036
7. Henning, A. M., Watt, J., Miedziak, P. J. et al. Gold-Palladium Core-Shell Nanocrystals with Size and Shape Control Optimized for Catalytic Performance. Angew Chem Int Edit, 2013, 52 (5), 1477-1480. https://doi.org/10.1002/anie.201207824
8. Tang, M., Mao, S., Li, M., et al. RuPd alloy nanoparticles supported on N-doped carbon as an efficient and stable catalyst for benzoic acid hydrogenation. ACS catalysis, 2015, 5(5), 3100-3107. https://doi.org/10.1021/acscatal.5b00037
9. Kordouli, E., Pawelec, B., Kordulis, C., et al. Hydrodeoxygenation of phenol on bifunctional Ni-based catalysts: Effects of Mo promotion and support. Applied Catalysis B: Environmental, 2018, 238, 147-160. https://doi.org/10.1016/j.apcatb.2018.07.012
10. Babu, N. S., Lingaiah, N., Prasad, P. S. Characterization and reactivity of Al_2O_3 supported Pd-Ni bimetallic catalysts for hydrodechlorination of chlorobenzene. Applied Catalysis B: Environmental, 2012, 111, 309-316. https://doi.org/10.1016/j.apcatb.2011.10.013
11. Ambursa, M. M., Juan, J. C., Yahaya, Y., et al. A review on catalytic hydrodeoxygenation of lignin to transportation fuels by using nickel-based catalysts. Renewable and Sustainable Energy Reviews, 2021, 138, 110667. https://doi.org/10.1016/j.rser.2020.110667
12. Zhang, J. W., Sun, K. K., Li, D. D., et al. Pd-Ni bimetallic nanoparticles supported on active carbon as an efficient catalyst for hydrodeoxygenation of aldehydes. Applied Catalysis A: General, 2019, 569, 190-195. https://doi.org/10.1016/j.apcata.2018.10.038

13. Li, J., Fan, J., Ali, S., et al. The origin of the extraordinary stability of mercury catalysts on the carbon support: the synergy effects between oxygen groups and defects revealed from a combined experimental and DFT study. Chinese Journal of Catalysis, 2019, 40(2), 141-146. https://doi.org/10.1016/S1872-2067(19)63271-7

14. Ding, W., Li, H., Zong, R., et al. Controlled hydrodeoxygenation of biobased ketones and aldehydes over an alloyed Pd–Zr catalyst under mild conditions. ACS Sustainable Chemistry & Engineering, 2021, 9(9), 3498-3508. https://doi.org/10.1021/acssuschemeng.0c07805

15. Zhu, J., Huang, Y., Mei, W., et al. Effects of intrinsic pentagon defects on electrochemical reactivity of carbon nanomaterials. Angewandte Chemie International Edition, 2019, 58(12), 3859-3864. https://doi.org/10.1002/anie.201813805

16. Wang, J. X., Cao, J. P., Zhao, X. Y., et al. Enhancement of light aromatics from catalytic fast pyrolysis of cellulose over bifunctional hierarchical HZSM-5 modified by hydrogen fluoride and nickel/hydrogen fluoride. Bioresource technology, 2019, 278, 116-123. https://doi.org/10.1016/j.biortech.2019.01.059

17. Kumar, R., Kumar, K., Pant, K. K., et al. Tuning the metal-support interaction of methane tri-reforming catalysts for industrial flue gas utilization. International Journal of Hydrogen Energy, 2020, 45(3), 1911-1929. https://doi.org/10.1016/j.ijhydene.2019.11.111

18. Fan, R., Li, Z., Wang, Y., et al. Promotional effect of ZrO_2 and WO_3 on bimetallic Pt-Pd diesel oxidation catalyst. Environmental Science and Pollution Research, 2022, 29(4), 5282-5294. https://doi.org/10.1007/s11356-021-15800-7

19. Kerkar, R. D., Salker, A. V. Synergistic effect of modified Pd-based cobalt chromite and manganese oxide system towards NO-CO redox detoxification reaction. Environmental Science and Pollution Research, 2020, 27(21), 27061-27071. https://doi.org/10.1007/s11356-020-09146-9

20. Li, R., Huang, Y., Zhu, D., et al. Improved oxygen activation over a carbon/Co_3O_4 nanocomposite for efficient catalytic oxidation of formaldehyde at room temperature. Environmental Science & Technology, 2021, 55(6), 4054-4063. https://doi.org/10.1021/acs.est.1c00490

21. Zhao, L., Zhao, J., Wu, T., et al. Synergistic effect of oxygen vacancies and Ni species on tuning selectivity of Ni/ZrO_2 catalyst for hydrogenation of maleic anhydride into succinic anhydride and γ-butyrolacetone. Nanomaterials, 2019, 9(3), 406. https://doi.org/10.3390/nano9030406

22. Xu, H., Xue, M., Huang, G. Characterization of Ni-Ce/N-rGO catalyst and its performance in catalytic hydrogenation of phenol to cyclohexanone. Acta Petrolei Sinica (Petroleum Processing Section), 2022, 39(1), 120-126.

23. Miao, C., Zhou, G., Chen, S., et al. Synergistic effects between Cu and Ni species in NiCu/γ-Al_2O_3 catalysts for hydrodeoxygenation of methyl laurate. Renewable Energy, 2020, 153, 1439-1454. https://doi.org/10.1016/j.renene.2020.02.099

24. Li, A., Shen, K., Chen, J., et al. Highly selective hydrogenation of phenol to cyclohexanol over MOF-derived non-noble Co-Ni@NC catalysts. Chemical Engineering Science, 2017, 166, 66-76. https://doi.org/10.1016/j.ces.2017.03.027

25. Lee, J. S. M., Fujiwara, Y. I., Kitagawa, S., et al. Homogenized bimetallic catalysts from metal–organic framework alloys. Chemistry of Materials, 2019, 31(11), 4205-4212. https://doi.org/10.1021/acs.chemmater.9b01093

26. van der Hoeven, J. E., Jelic, J., Olthof, L. A., et al. Unlocking synergy in bimetallic catalysts by core–shell design. Nature materials, 2021, 20(9), 1216-1220. https://doi.org/10.26434/chemrxiv.13218155

27. Wang, Y., Wang, Z., Xu, C., et al. Synthesis of alumina supported Pt-SnO2 hybrid nanostructures by in situ transformation of PtSn alloy nanoparticles and their application as highly efficient catalysts for selective hydrogenation of furfural. The Journal of Physical Chemistry C, 2023, 127(8), 4033-4041. https://doi.org/10.1021/acs.jpcc.2c07661

28. Gao, X., Tian, S., Jin, Y., et al. Bimetallic PtFe-catalyzed selective hydrogenation of furfural to furfuryl alcohol: solvent effect of isopropanol and hydrogen activation. ACS Sustainable Chemistry & Engineering, 2020, 8(33), 12722-12730. https://doi.org/10.1021/acssuschemeng.0c04891

29. Zhang, P., Liu, C. H., Chen, L., et al. Factors influencing the activity of SiO2 supported bimetal Pd-Ni catalyst for hydrogenation of α-angelica lactone: oxidation state, particle size, and solvents. Journal of Catalysis, 2017, 351, 10-18. https://doi.org/10.1016/j.jcat.2017.04.017

30. Fan, R., Chen, C., Han, M., et al. Highly dispersed copper nanoparticles supported on activated carbon as an efficient catalyst for selective reduction of vanillin. Small, 2018, 14(36), 1801953. https://doi.org/10.1002/smll.201801953

31. Yang, F., Liu, D., Zhao, Y., et al. Size dependence of vapor phase hydrodeoxygenation of m-cresol on Ni/SiO2 catalysts. ACS catalysis, 2018, 8(3), 1672-1682. https://doi.org/10.1021/acscatal.7b04097

32. Alam, M. I., Khan, T. S., Haider, M. A. Alternate biobased route to produce Î-decalactone: elucidating the role of solvent and hydrogen evolution in catalytic transfer hydrogenation. ACS Sustain Chem Eng, 2019, 7, 2894–2898. https://doi.org/10.1021/acssuschemeng.8b05014

33. Liu, S., Simonetti, T., Zheng, W., et al. Selective hydrodeoxygenation of vegetable oils and waste cooking oils to green diesel using a silica-supported Ir–ReOx bimetallic catalyst. ChemSusChem, 2018, 11(9), 1446-1454. https://doi.org/10.1002/cssc.201800321

34. Zhang, X., Du, Y., Jiang, H., et al. Insights into the stability of Pd/CN catalyst in liquid phase hydrogenation of phenol to cyclohexanone: role of solvent. Catalysis Letters, 2019, 149, 3087-3096. https://doi.org/10.1007/s10562-019-02844-1

35. You, H., Lin, J., Huang, K. Mechanism of solvent effect on hydrogenation of lignin phenolic compounds. CIESC Journal, 2022, 73 (10), 4498-4506. https://doi.org/10.11949/0438-1157.20220826

36. Panagiotopoulou, P., Martin, N., Vlachos, D. G. Effect of hydrogen donor on liquid phase catalytic transfer hydrogenation of furfural over a Ru/RuO$_2$/C catalyst. Journal of Molecular Catalysis A: Chemical, 2014, 392, 223-228. https://doi.org/10.1016/j.mol-cata.2014.05.016

37. Zhang, L., Pu, M., Lei, M. Hydrogenation of CO$_2$ to methanol catalyzed by a manganese pincer complex: insights into the mechanism and solvent effect. Dalton Transactions, 2021, 50(21), 7348-7355. https://doi.org/10.1039/D1DT01243F

38. Wang, Y. H., Khudaida, S. H., Ong, J. Y., et al. Improved Design of Maximum-Boiling Phenol/Cyclohexanone Separation with Experimentally Verified Vapor–Liquid Equilibrium Behaviors. Industrial & Engineering Chemistry Research, 2020, 59(13), 6007-6020. https://doi.org/10.1021/acs.iecr.0c00042

39. Liu, Y., Guo, W., Lu, X., et al. Density functional theory study of hydrogenation of S to H$_2$S on Pt–Pd alloy surfaces. RSC advances, 2016, 6(8), 6289-6299. https://doi.org/10.1039/C5RA20087C